JOURNAL OF MATERIALS SCIENCE 30 (1995) 173–178

Micromechanism of fracture in Al/SiC composites

X. GE*, S. SCHMAUDER
Max-Planck-Institut fur Metallforschung, Institut fur Werkstoffwissenschaft, Seestrasse 92, Stuttgart, Germany

An SEM study was made of the micromechanism of fracture in SiC particle-reinforced 6061 aluminium composites. The fracture toughness tests on the composites with SiC volume fractions of 0%, 10% and 20% were conducted on single-edge notched sheet specimens. Both qualitative observations of void nucleation at the notch root of the composite samples and quantitative measurements of crack profiles are made to assess the special role of the particle effects in these composites. The results are discussed with respect to the micromechanism of particle breakage and interface debonding and their effect on the nucleation and propagation of microcracks. Two kinds of void are defined to explain the facts that Al/SiC is brittle macroscopically and ductile microscopically. The direction of crack propagation in Al/SiC and the microstructure in the tip region of the crack are also studied with these results.

1. Introduction

Engineering materials with a discontinuous second phase as a toughener [1] or reinforcement [2] have been widely studied in materials science and engineering. Investigations of the fracture characteristics of SiC particle-reinforced aluminium have shown that particle addition usually lowers the fracture toughness [3–5]. Reported fracture toughness values for unreinforced aluminium alloys are in the range of 25–75 MPa $m^{1/2}$, while the composites have plane strain toughness values of 7–25 MPa $m^{1/2}$ [6, 7]. Many researchers have shown that the effect of microstructure on the fracture toughness is significantly affected by the details of the matrix microstructure, interface characteristics, and degree of clustering in the materials [8–9]. However, SEM fractography has revealed that the fracture surface consists of microvoids, corresponding to ductile fracture with dimples [10]. The sources of these dimples have been attributed to fracture of SiC particles [11], inclusions and precipitates or decohesion from the matrix as well as matrix failure [12, 13]. An attempt to explain these special failure characteristics of Al/SiC composite materials, which behave macroscopically brittle, but microscopically ductile, was the main purpose of this work. The fracture toughness tests on the composites were carefully designed with single-edge notched sheet (SENS) [14] specimens in the SEM. Both qualitative observations of void nucleation and quantitative measurements of crack profiles were made to assess the specific role of the particle-reinforcement mechanism in the composites. The microstructure analysis is proposed to understand and explain the particle effects during the crack initiation and propagation in these composites.

2. Experimental procedure

The composites used consisted of particle-reinforced aluminium alloy 6061 manufactured by extruding mixtures of aluminium powder and SiC particles. The volume fractions of particles in the composites were 0%, 10% and 20%. The mechanical properties of these composites are shown in Table I. Distributions of measured SiC particle diameters are shown in Fig. 1a and b.

The SENS sample was designed according to the requirements of the SEM machine. The dimensions of the sample are shown in Fig. 2. The test was carried out in a Jeol JSM-35 scanning microscope. The machine automatically records the applied load versus displacement curves, and the monitor is used to examine the tip of the notch to understand the notch deformation, as well as nucleation, growth and coalescence of voids during loading. A record of the process is made by a video recorder.

3. Results

3.1. Qualitative observations of void nucleation

General observations were made on the tip and root of the notch during the loading process. Voids nucleated in the middle of the notch root, as observed in the SEM, at K_0/K_I equal to 0.68, 0.784, and 0.85 for 0%, 10% and 20% SiC volume fraction composites,

Present address: East China University of Science and Technology, Shanghai, People's Republic of China.

0957–4530

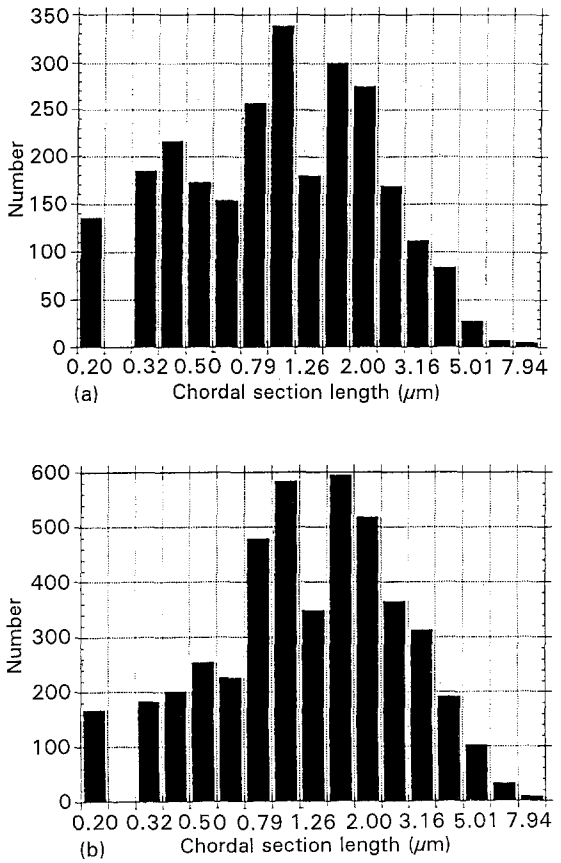

Figure 1 Distributions of particle diameters. (a) 10% Al/SiC, (b) 20% Al/SiC (courtesy J. Wulf).

TABLE I Mechanical properties of Al/SiC composites used in the test[a]

Matrix	SiC particle (vol %)	Heat treatment[b]	Yield strength, σ_y (MPa)	Ultimate strength, σ_u (MPa)	Elastic modulus, E_c (GPa)
6061	0	T6	368.5	394	71.7
6061	10	T6	381.2	420	90.5
6061	20	T6	397	458	107.8

[a] Data in Table I are from Kobe-Steel Corporation.
[b] T6 heat treatment: solution treated at 803 K for 2 h, water quenched, aged at 448 K for 8 h and air cooled.

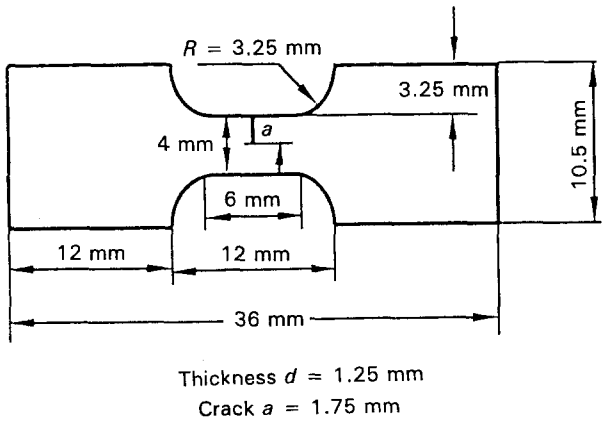

Figure 2 Dimensions of SENS specimen.

respectively, where K_I is the stress intensity factor of the sample calculated according to Brown and Srawley [15] and K_0 is the fracture toughness. Measured data of K_0 and K_I are shown in Table II.

During loading, the first void was observed in the centre of the notch root, Figs 3 and 4. Fig. 3 shows a stage of void growth at the notch root (arrows 1, 2, 3) as well as plastic deformation in the tip region of the notch in 0% SiC composites (arrow a). Fig. 4a shows void nucleation and growth in a 10% SiC composite sample. When the voids grow at the root of the notch, two possibilities exist for void growth to cause microcrack initiation in the adjacent free surface: one arises at the nearest point to the void in the free surface, characterizing the high stress concentration in the notch tip (point a); another, about 120 μm away, will form a microcrack (point b). As the loading increases, the voids at the notch root grow and coalesce towards the microcrack and combine directly with the microcrack. (Fig. 4b). Fig. 4c is the picture of a local amplification of point c in Fig. 4b, showing the crack propagation. Fig. 4d shows the propagation of the main crack. The crack in the Al/20% SiC sample propagates so rapidly that it is difficult to record more detail during loading.

3.2. Quantitative measurements of COD curves

CODs of the notch and $2u(x)$ were measured for the specimens, where x is the distance behind the notch tip

TABLE II Fracture toughness of Al/SiC composites[a]

	0% SiC	10% SiC	20% SiC
K_I (MPa m$^{1/2}$)	38.7	25.76	22
K_0 (MPa m$^{1/2}$)	26.4	20.2	18.9
K_0/K_I	0.68	0.784	0.85

[a] K_I and K_0 are calculated from [15].

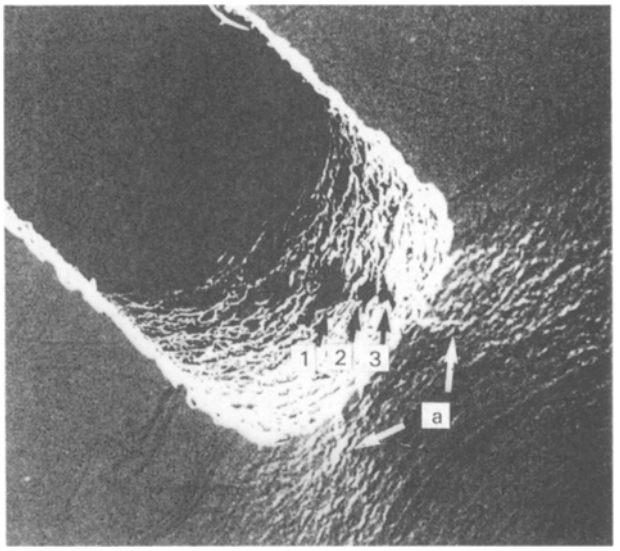

Figure 3 Scanning electron micrograph of void nucleation, growth and coalescence in the notch root surface of a pure aluminium sample.

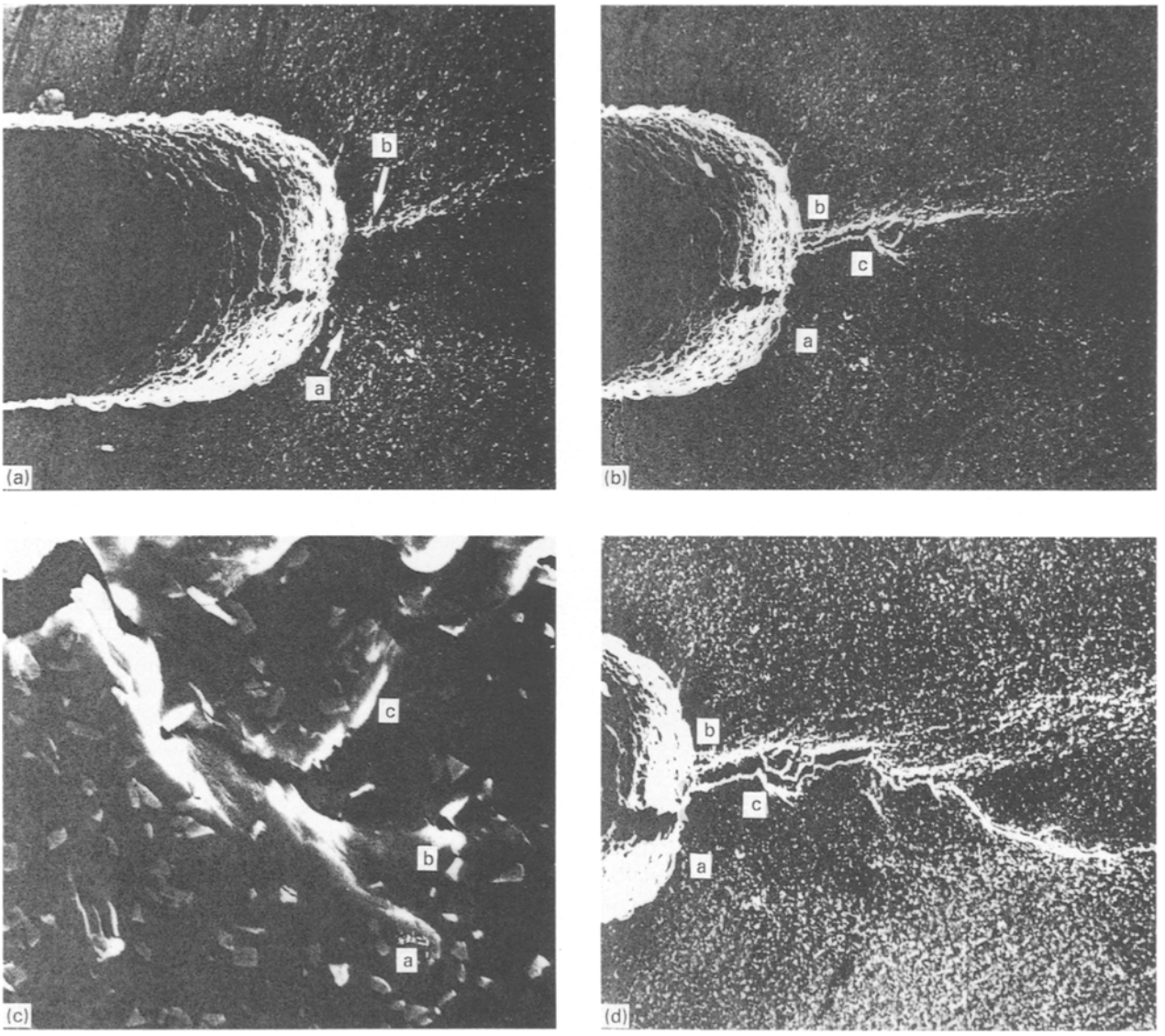

Figure 4 Scanning electron micrographs of void nucleation, growth and coalescence in Al/10% SiC. (a) Void nucleation, growth and coalescence, (b) void coalescence and crack initiation, (c) local magnification of point c in (b), (d) the main crack propagation.

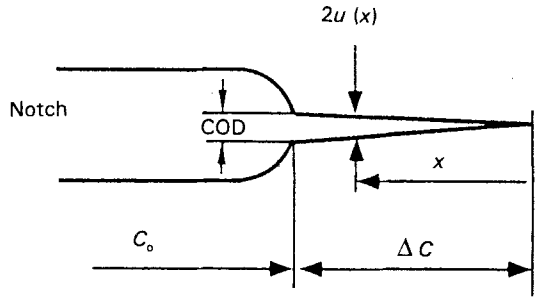

Figure 5 Schematic drawing of the SENS specimen. Notch length C_0, crack extension ΔC, crack profile by COD, $2u(x)$ at a distance behind the crack tip.

as indicated in Fig. 5. The results are directly measured from the scanning electron micrographs and are shown in Fig. 6. The crack propagation profile is that associated with a plane stress crack with the correlated applied stress intensity factor, K_I [16]

$$u(x) = 8\left[\frac{K_I}{(2\pi)^{1/2}E}\right]^{x^{1/2}} \quad (1)$$

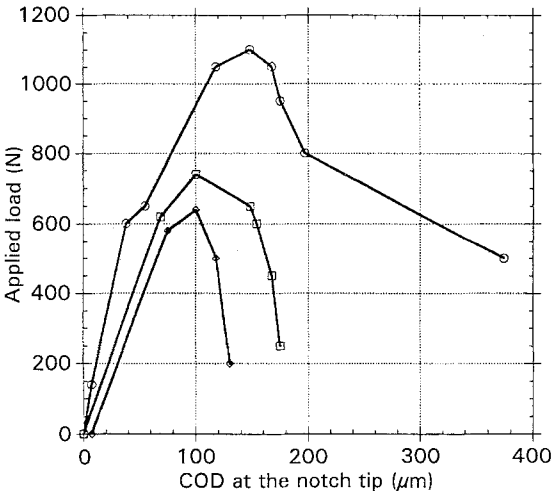

Figure 6 Crack opening displacement versus applied load curves. (○) 0% SiC, (□) 10% SiC, (◇) 20% SiC.

where K_I is shown in Table II and E is Young's modulus of the composites from Table I. Equation 1 is plotted together with experimental data in Fig. 7. The experimental data are lower than that predicted by

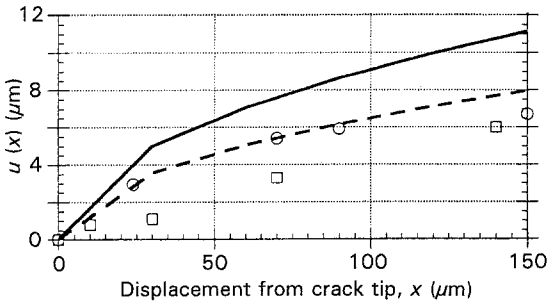

Figure 7 Comparison between (—, - - -) prediction from Equation 1 and (○, □) experimental data of the crack profile for (—, ○) 10% SiC and (- - -, □) 20% SiC.

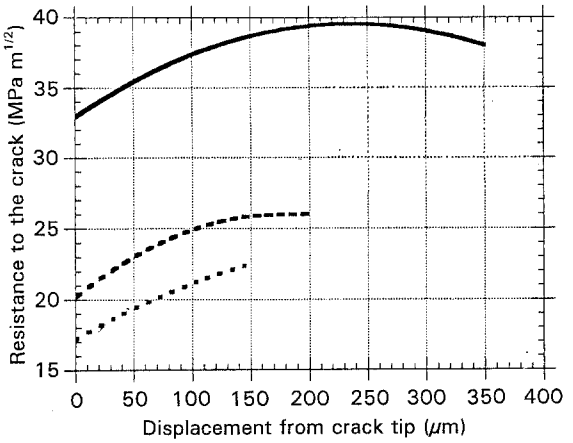

Figure 8 Crack resistance curves for Al/SiC composites: (—) 0% SiC, (— — —) 10% SiC, (- - -) 20% SiC.

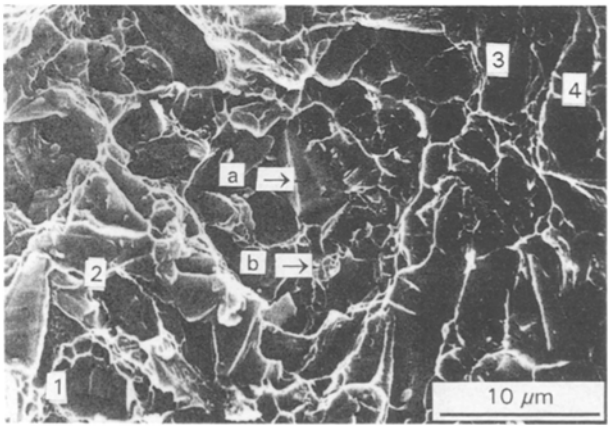

Figure 9 Scanning electron micrograph showing the properties of the primary and secondary voids.

Equation 1. Fig. 8 is the stress intensity factor for three composites measured behind the crack tip during the *R*-curve determination.

3.3. Primary and secondary voids

Void nucleation is significantly altered when the particles are present. From Fig. 9, there are at least two kinds of void observable in the fracture surface of Al/SiC composites. The first kind of void nucleates either at broken particles or at decohering interfaces

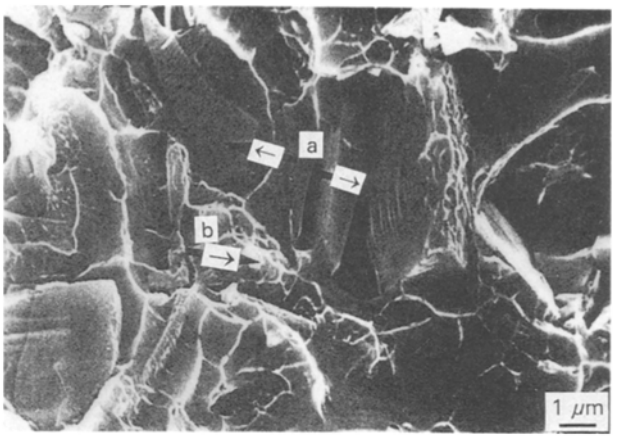

Figure 10 Scanning electron micrograph of primary and secondary voids.

(point a). Both the size and shape of voids are found to be associated with the SiC particles [11], and this is called a primary void. Therefore, the surface of these voids characterizes cleavage (Fig. 10, point a). The other kind of void is nucleated in the matrix ligaments between the particles. The dimensions of these voids are about 0.3–1.2 μm for Al/20% SiC composites, as shown in Fig. 10. From Fig. 10, point b, it can be seen that these voids are constrained by interface bond forces around them and their sizes are very small compared with the primary void. These voids are termed secondary voids. They are dimples and characterize microscopic ductility. However, these void dimensions are affected significantly by particle size, volume fractions, and interface properties.

4. Discussion

In Table II, K_0 is the toughness when a void nucleates as observed in SEM, and K_I is the stress intensity factor of the material. K_0/K_I can be used to express the fracture behaviour of the composites. When a void nucleates and grows, the material can still sustain additional applied loading if $K_0 < K_I$. When K_0/K_I is smaller, i.e. the stages of void nucleation, growth and coalescence are longer, the composites show ductile behaviour. If K_0/K_I increases, and tends to 1 as the SiC particle volume fraction increases, the effect of void nucleation, growth and coalescence decreases, and the material becomes brittle. In Fig. 6 the notch opening displacement decreases rapidly as particle volume fractions increase. When the voids nucleate and grow at the notch root, the curve of load versus notch opening displacement does not change its shape markedly until the voids coalesce to microcrack, particularly in the curve of pure aluminium in Fig. 6. Equation 1 is used to describe the crack profile. Compared with curves in Fig. 7 and the data measured in the test, all data points are obviously lower than predicted by Equation 1, which states the real length of the crack in Al/SiC composites is longer than that given by Equation 1, and shows the brittle nature of the materials. Fig. 8 shows the *R*-curve of these composites in the plane stress state. The resistance to the crack propagation in pure aluminium is about

twice that of Al/20% SiC. During practical tensile tests, the curve of applied load versus displacement characterizes ductile features for pure aluminium samples and brittle features for Al/20% SiC samples. When an applied load reaches a certain criterion value, the crack initiates at the tip of the notch and rapidly propagates in Al/20% SiC samples. This situation is very similar to crack growth in ceramic matrix composites [17].

During the tensile test, more detailed examinations of Al/10% SiC in the SEM were made of void nucleation, growth and coalescence, as well as the crack initiation. The void was first observed at the symmetry plane of the notch root surface (Fig. 4a) because there is a high stress constraint region. As the loading increases, the first void nucleates and grows and then the second and third voids are observed (Fig. 4b). Similar situations are found in Fig. 3 in the notch root of pure aluminium. Comparing Fig. 3 with Fig. 4a, although there is the same number of the voids observed between the centre of the notch root and the free surface in these two materials, the size of the voids is very different. The maximum size is about 20 μm for pure aluminium, 5 μm for Al/10% SiC. The ratio of both void sizes is 4. The deformation of the materials has been altered by the particles in the matrix, so the void size becomes small and the composite is brittle. But voids are not observed in the free surface of the notch tip region in Figs 3 and 4. When loading increases, the voids coalesce at the notch root, and at the same time microcracks initiate in the free surface of the notch tip. The shear failure near the notch root and free surface can be observed in Fig. 4b.

After voids coalesce and microcracking initiates, the main crack will be formed. The crack meanders microscopically whereas the failed surface is flat macroscopically, more so when the SiC volume fraction increases. Although apparently easy paths for crack propagation can develop early in the high straining process, the main crack does not necessarily follow these routes. The crack propagation is mainly affected by the microstructure of the composites. Fig. 4c indicates three possibilities for crack propagation: point a is a stress concentration region caused by a small group of cluster particles; point b shows interface debonding in the tip region of the crack; point c is a possible way to form the secondary crack connected with the main crack. The crack will follow the direction of the easiest propagation. Finally, the crack goes along the point c direction in Fig. 4d. There are two reasons to explain why the crack follows this route. On the top right in Fig. 4c, the direction of the crack has been influenced to turn left by interface debonding at the left tip region of the crack, which has inclined to the maximum principal strain direction, so it is reasonable for the crack to turn back to the original line; on the bottom right in Fig. 4c, a larger debonding is formed. The influence of this debonding on the crack path is greater than that of points a and b. The crack propagation in Al/SiC composites can be described as follows: first, the voids nucleate, grow and coalesce at the notch root, and a microcrack initiates at the tip of the notch in the free surface; then the voids coalesce and connect with the microcrack to form the main crack; third, the debonding or particle breakage in the tip region of the crack occur before the crack advances; these debonding or broken particles coalesce with the crack, and the crack propagates.

Observed primary and secondary voids have been shown to explain exactly why the Al/SiC composites depict microscopically ductile features. The primary voids associate with particles, and the particle can be found to be located inside the primary void in Figs 9 and 10. The sources of primary voids are the interface debonding or the cracked particles. Points 1 and 2 in Fig. 9 show that both the size and shape of the voids are associated with the SiC particles in it. Points 3 and 4 in Fig. 9 show the primary voids for particles that may be in the opposite fracture surface. From point a in Fig. 10, there are cracked particles, showing typical cleavage fracture. It is reported that the particles will crack at a relatively low strain level [18, 19]. The stress triaxial constraint around the particle makes the matrix harder than in the absence of particles. The linear elastic part of this constraint has been analysed theoretically and quantitatively [20]. The reason for debonding and breakage of particles at the tip of the notch can be explained by the high constraint effect of triaxial stress [21]. HREM analysis of the interface in Al/SiC with T6 heat treatment shows the brittle Al_4C_3 precipitates [22]. So the primary void characterizes the brittle property of composites. Secondary voids occur in the spacing between particles during loading. These voids follow three stages of nucleation, growth and coalescence. However, the dimensions of these voids are very small (Fig. 9), and they can only be examined clearly by magnifying more than 1000 times in the SEM. Secondary voids, which show many small dimples in the fracture surface and behave in a ductile manner, depend on the spacing of particles and interface stress constraint. These regions are under a strong deformation constraint and plastic strain associated with void formation is smaller. For these reasons, the processes of nucleation, growth and coalescence of the secondary voids are then too small to exhibit tensile plastic features of the material. The low fracture toughness of these composites is mainly determined by primary voids and characterized as brittle events, while secondary voids have little influence on the ductile behaviour of the materials.

Because of the high stress concentration at the tip of the crack, interface debonding and particle cracking develop prior to the main crack arrival. Fig. 11 shows the region of the crack tip containing many broken particles and interface debondings, which will have a great effect on the crack paths. Fig. 11a shows the debonding or broken particles in this region of Al/20% SiC. Fig. 11b depicts the debonding and broken particles near the failed fracture surface. The arrows in Fig. 11 gives the direction of crack propagation. This microstructural region ahead of the main crack experiences the rapid propagation conditions for macrocracks, and affects the crack path, although macroscopically the main crack follows the directions that the maximum principal stress would predict as shown in Fig. 4d. This is why the crack propagates so

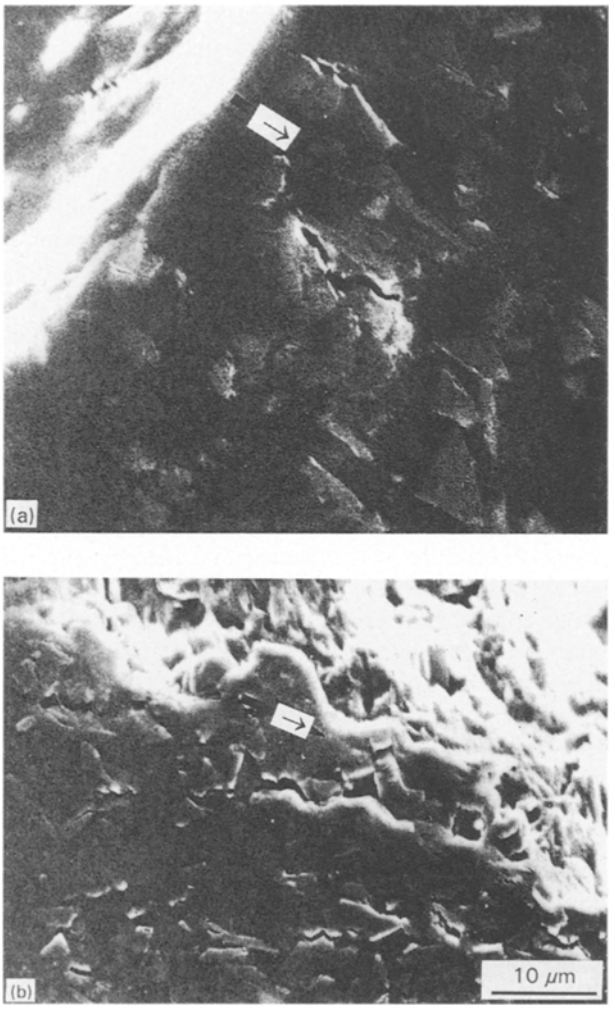

Figure 11 Debonding and broken particles in Al/20% SiC: (a) in the notch tip region, (b) near the failed crack surface.

rapidly in Al/20% SiC samples in the test. The many debonding and broken particles in this region of the crack tip is the main reason for the brittle fracture and, hence is responsible for the low ductility of the composite materials. However, it is not yet clear quantitatively at what applied strain level, particle cracking occurred and which of the two types of behaviour, interface debonding or particle cracking, is predominant.

5. Conclusions

1. K_0/K_I can be used to express material toughness. K_0/K_I is equal to 0.68, 0.784 and 0.85 for 0%, 10% and 20% Al/SiC materials. If K_0 tends toward K_I, the material toughness becomes lower.

2. Two kinds of void have been defined according to the properties of the voids in the fracture surface. The primary voids govern the brittle property of composites, while the secondary voids, governing the ductile property, have little influence on the fracture toughness.

3. The voids initially nucleate, grow and coalesce at the notch root surface. The crack propagation observed in the free surface of the samples is associated with debonding and particle cracking in the tip region of the crack.

4. The direction of crack propagation depends on the microstructure in the tip of the crack, and macroscopically on the maximum principal strain direction.

Acknowledgements

One of the authors, GE, thanks DAAD/K.C. Wong fellowship for support while working at MPI. Helpful discussions, with Dr Alexander Wanner, particle diameter distribution measurements conducted by Mr J. Wulf and Mrs I. Morlok, are gratefully acknowledged.

References

1. D. B. FLINN, M. RUHLE and A. G. EVANS, *Acta Metall.* **37** (1989) 3001.
2. X. GE, D. ZHANG and D. JU, in "Advances in Constitutive Laws for Engineering Materials" Vol. 1, edited by J. Fan and S. Murakami (International Academic Publishers, Chongging, China, 1989) p. 497.
3. S. V. NAIR, J. K. TIEN and R. C. BATES, *Int. Metal. Rev.* **30** (1985) 275.
4. A. D. DIVECHA, S. G. FISHMAN and S. D. KAMARKAR, *J. Metals* **33** (1981) 12.
5. A. D. DIVECHA and S. G. FISHMAN, *SAMPE Q.* April (1981) 40.
6. D. L. DAVIDSON, *Metall. Trans.* **22A** (1991) 113.
7. B. ROEBUCK and J. D. LORD, *Mater. Sci. Technol.* **6** (1990) 1199.
8. M. J. BIRT and W. S. JOHNSON, in "Fundamental Relationship between Microstructure and Mechanical Properties of Metal Matrix Composites", edited by P. K. Liaw and M. N. Gungor, (MMS, California, USA, 1990) p. 71.
9. A. K. VASUDEVAN, O. RICHMOND, F. ZOK and J. D. EMBURY, *Mater. Sci. Eng.* **A107** (1989) 63.
10. J. J. LEWANDOWSKI, C. LIU and W. H. HUNT, Jr. *ibid.* **A107** (1989) 241.
11. P. MUMMERY and B. DERBY, in "Fundamental Relationship between Microstructure and Mechanical Properties of Metal Matrix Composites", edited by P. K. Liaw and M. N. Gungor (MMS, 1990) p. 161.
12. C. A. HANDWERKER, M. D. VANDIN, U. R. KATTNER, and D. J. LEE, in "Metal-Ceramic Interface", *Acta-Scripta Metall. Proc. Ser 4*, edited by M. Ruhle, A. G. Evans, M. F. Ashby and J. P. Hirxx (Pergamon Press, Oxford, 1990) p. 129.
13. J.-D. LEE, M. D. VANDIN, C. A. HANDWERKER, and U. R. KATTNER, in "High Temperature/High Performance Composites", edited by F. D. Lemkey, S. G. Fishman, A. G. Evans and J. R. Strife (MRS, Pittsburgh, USA, 1988) p. 357.
14. W. A. LOGSDON and P. K. LIAW, *Eng. Fract. Mech.* **24** (1986) 737.
15. W. F. BROWN Jr and J. E. Srawley, ASTM STP 40 (American Society for Testing and Materials, Philadelphia, PA, 1966).
16. J. RUDEL, J. F. KELLY and B. R. LAWN, *J. Am. Ceram. Soc.* **73** (1990) 3313.
17. X. GE, D. ZHANG and D. JU, *Proc. ICCM-7* **4** (1989) 36.
18. H. LAGACE and D. J. LLOYD, *Can. Metall. Q.* **28** (1989) 145.
19. Z. WANG, and R. J. ZHANG, *Metall. Trans.* **22A** (1991) 1585
20. X. GE and S. SCHMAUDER, *Mater. Sci. Eng.* **A168** (1993) 93–97.
21. M. H. POECH and H. F. FISCHMEISTER, *Acta Metall. Mater.* **40** (1992) 487.
22. M. VAN DEN BURG and J. TH. M. DE HOSSON, *Acta Metall. Mater.* **40** *Suppl.* (1992) 281.

Received 30 September 1993
and accepted 16 June 1994